International Journal of Structural Stability and Dynamics
Vol. 17, No. 5 (2017) 1740011 (15 pages)

DOI: 10.1142/S0219455417400119

World Scientific
www.worldscientific.com

Influence of Impulse Force Loading on Vibrations of the Collecting Electrodes

Andrzej Nowak* and Paweł Nowak†

Department of Transport and Informatics, University of Biesko-Biała
2 Willowa Street, Bielsko-Biała, 43-300, Poland
**a.nowak@ath.bielsko.pl*
†*pnowak@ath.bielsko.pl*

Jan Awrejcewicz

Department of Automation, Biomechanics and Mechatronics,
Łódz University of Technology 1/15 Stefanowski Street, Łódz, 90-924, Poland
and Institute of Vehicles, Warsaw University of Technology,
84 Narbutta Street, Warsaw, 02-524, Poland
jan.awrejcewicz@p.lodz.pl

Received 3 March 2016
Accepted 4 August 2016
Published 9 January 2017

Results of the simulations of vibrations of collecting electrode system of dry electrostatic precipitator (ESP) are reported. The system of nine electrodes 16 m long, suspension beam (upper beam) and anvil beam (bottom beam) is analyzed. First, the variants regarding differ position of the anvil beam are analyzed. Second, the differ position of a point of the impulse force as well as direction of the impulse force are investigated (in this case the anvil beam is in a "classic" position). Discretization of both beams and electrodes is carried out employing the modified rigid finite element method (RFEM). It allows to study an influence of the mass distribution and geometric properties of the analyzed system. Moreover, the method is convenient for the introduction of additional lumped mass parameters modeling the joints that fasten the electrodes to the suspension beam, distance-marking bushes, riveted and screw joints, etc. Position of the anvil beam and position/direction of the point of impulse force application can have essential influence on tangent and normal accelerations at different points of the plates, and thus on the effectiveness of the dust removal process. We aim to find optimal position of an anvil beam, which guaranties the maximum amplitudes of vibrations and their proper distribution in the plates.

Keywords: Rigid finite element method; electrostatic precipitator; analysis of vibrations.

1. Introduction

Particulate matter emitted by power and industrial plants consists of a polydisperse particulate. It constitutes a group of particles of different size, from submicron

particles to particles of a diameter of several tens μm.[1] Particle size distribution is affected by both the pollution generated by the same source and the efficiency of the used dust collector.[2] Modern electrostatic precipitators, thanks to their high total dust extraction efficiency reaching 99.9%, are used for a thorough purification of gases coming from dust particles. A scheme of a single-sectional electrostatic precipitator is demonstrated in Fig. 1.

The basic elements of currently built ESP are: a set of emitting electrodes **2**, a set of collecting electrodes **3**, electric power system **1** and housing with supply **4**, and discharge **5** conduits for the gas yielded by the dust collector. The dust is discharged using channel **6**. The interior of a dry ESP is a complex steel structure. It consists of multiple, repetitive subassemblies, called sections of collecting electrodes [Fig. 2(a)]. Sectioning of the ESP is applied in the case of dust extraction of large volumes of gas. A single section is formed by up to several tens of collecting electrodes, separated alternately with the sets of discharge electrodes [Fig. 2(b)].

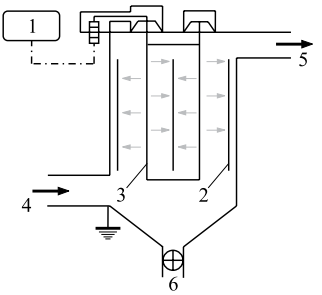

Fig. 1. Schematic representation of a single-sectional electrostatic precipitator.

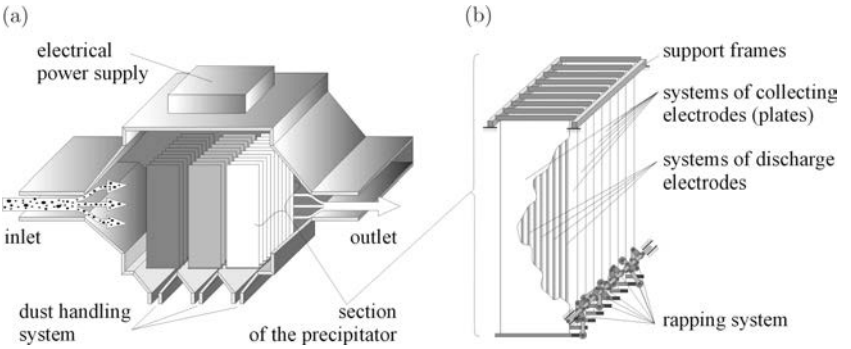

Fig. 2. Schematic representation of a three-sectional dry ESP (a) and a section of collecting electrodes (b).

The effective operation of an ESP is mostly dependent on the structure and proper selection of the profile of collecting electrodes.[3] One of the profiles, often used in domestic structures, is presented in Fig. 9(b). The systems of collecting electrodes are coupled with the sets of rappers, responsible for the removal of dust accumulated on these electrodes. In the case of ESP with a gravitational system of rappers, each section has its own drive shaft of rappers. The number of rappers corresponds to the number of the systems of collecting section electrodes. An important element of a rapping system, in terms of vibrations induced in the system of collecting electrodes, is a beater hanging on the arm rotated by a drive shaft (Fig. 3).

The removal of the particulate matter collected on the electrodes is yielded by oscillating accelerations allowing for the effective removal of particles coagulated on their surfaces. The analysis of the phenomena accompanying the operation of rapping devices, the improvement of reliability of the operation of rapping systems and the achievement of more efficient removal of particulate from collecting electrodes have been under investigation for many years.[4,5] Initially, the studies were based on physical models. A physical model of a dry ESP, which served to search for optimal parameters of rapping, expressed by the thickness of the particulate layer and the value of the generated acceleration only in two control points of collecting electrodes, have been given.[6] However, in the last decade, instead of building physical models of ESP, the dedicated and numerically advanced models are created, which serve to perform simulations either of a whole device[7] or only of its selected subassemblies.[8] The earlier works[9–12] present models allowing for a simulation of vibrations of electrodes, induced by an impulse force. The models were obtained using: the finite element method,[12] the slab strip method[9] and the rigid finite element method.[10,11] In the above-mentioned references, an emphasis is devoted to the validation of the models by comparing the results of measurements and computer simulations. The adopted compatibility criteria demonstrated that practically all of the applied methods give a satisfactory consistency of the results in the range of peak values of accelerations. It also applies to the RFEM, used in Ref. 13, and in the current study. Based on the models validated by measurements, an attempt was made to use the developed computer software to determine the effect of geometric and structural parameters of the electrode–rapper system aimed on the values of accelerations.

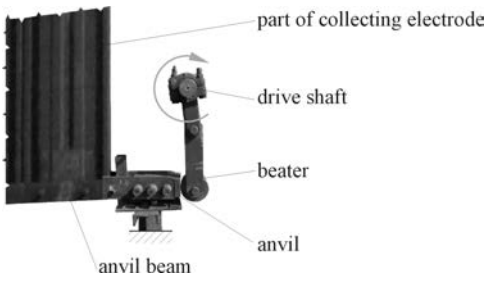

Fig. 3. Rapping system.

In the present paper, in addition to research presented in Ref. 13, the influence of different variants of loading of the impulse force is presented and discussed (see Sec. 3.2). The variants vary by a position of the point of impulse force application as well as direction of impulse force. The results of the conducted analyses are addressed to engineers and designers of ESP. The paper is organized in the following way. In Sec. 2, the RFEM model of the system of collecting electrodes as well as the model of the impulse force are presented. Next, in Sec. 3, the test calculations of the impact of position of the anvil beam in the system (Sec. 3.1) and the influence of different variants of loading of the impulse force (Sec. 3.2) are presented and discussed. Finally, in Sec. 4 some closing remarks are presented.

2. RFEM Model of a System of Collecting Electrodes

The RFEM is an original Polish method, developed since the 70s of the 20th century.[14,15] Its essential feature is a simple physical interpretation and numerical effectiveness, particularly in the area of the analysis of vibrations around the position of a static equilibrium. In the present study, the subject for modeling is a single set of collecting electrodes (Fig. 4) comprising a suspension beam (upper beam), on which p electrodes are hung (usually no more than 10), braced at the bottom by the anvil beam (bottom beam). An anvil beam is completed with an anvil, hit by the beater.

Based on the analysis of the shapes of collecting electrodes presented in the introduction, it can be noted that they consist of several long slab strips, connected at certain angles. This implies the way of their division into elements. The electrode k is associated with a coordinate system shown in Fig. 5.

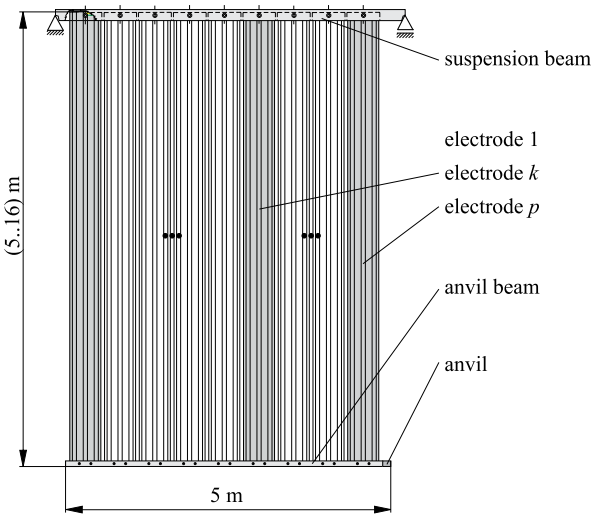

Fig. 4. The system of collecting electrodes.

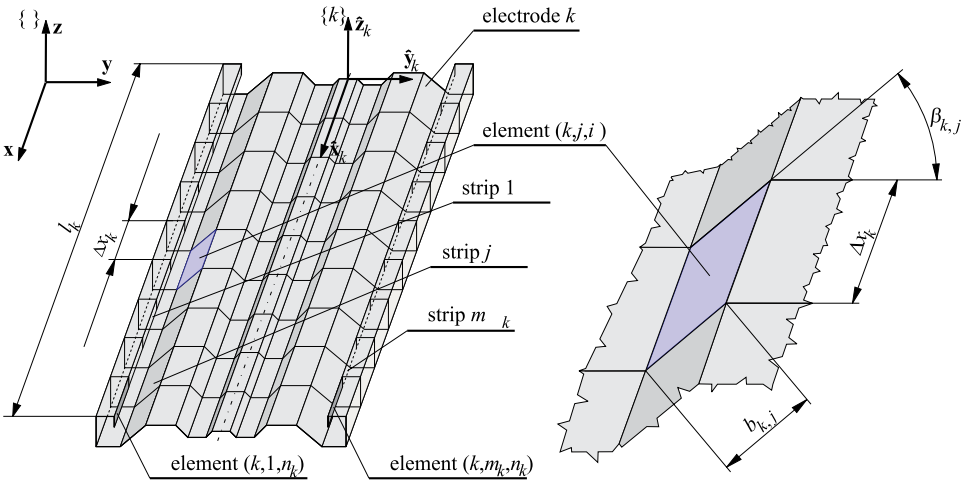

Fig. 5. Strip j with width $b_{k,j}$ and angle of inclination $\beta_{k,j}$ towards axis $\hat{y}$ ({} — global coordinate system, $\{k\}$ — local coordinate system connected with electrode k with axes parallel to those of system {}).

A single strip of an electrode has a constant width and thickness. It is assumed that the strips are numbered from 1 to m_k, while the extreme left-hand strip has number 1, and the extreme right-hand strip number m_k. In the direction $\mathbf{x}$ the strip is divided into n_k elements of the length:

$$\Delta x_k = \frac{l_k}{n_k}, \tag{2.1}$$

where l_k denotes a length of the electrode (and thus the length of strips counts from 1 to m_k). Therefore, the whole collecting electrode is divided into

$$n_e^{(k)} = m_k n_k \tag{2.2}$$

elements. It should be noted that the elements of the strip j of the electrode k are of the same size. The introduced division will serve to determine the energy of the elastic strain of the electrode element and its kinetic energy, using rectangular shell elements. In the RFEM the presented division is called a primary division. In the secondary division, primary elements are divided into four parts rigid finite elements (rfe), as shown in Fig. 6, and connected by means of spring-damping elements (sde).

In the present study spring-damping elements sde are placed similarly as in Ref. 16 and in contrast to Ref. 17. This way of sde arrangement provides the opportunity to consider the torsion of discretized plates and eliminates singularities in the model. Upper and lower beams are discretized in a similar way (Fig. 7).

After calculating mass parameters of rfe and stiffness coefficients of sde for plates and beams, the equation of motion can be presented in the general form

$$\mathbf{M}\ddot{\mathbf{q}} + \mathbf{C}\mathbf{q} = \mathbf{f}, \tag{2.3}$$

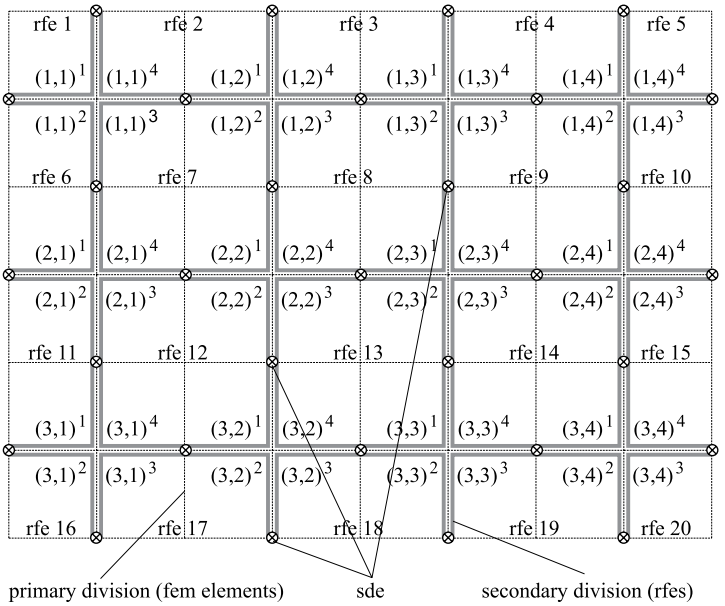

Fig. 6. Exemplary scheme of discretization in RFEM: primary (|) and secondary (||) divisions.

where: $\mathbf{M}$ is the mass matrix of constant elements, $\mathbf{C}$ is the stiffness matrix of constant elements, $\mathbf{q}$ denotes the vector of generalized coordinates, $\mathbf{f} = \mathbf{f}(\mathbf{q}, \mathbf{F})$ and $\boldsymbol{F}(t)$ are the forces applied to the anvil of the bottom beam (Fig. 8).

In Eq. (2.3) damping is omitted, as from the engineering point of view, it is important to determine the maximum possible acceleration values (the latter are obtained for system without damping). It should also be taken into account that in the structures of real ESP, the following factors are higher than material damping: damping of the structure and damping caused by the particulate accumulated on the electrodes.

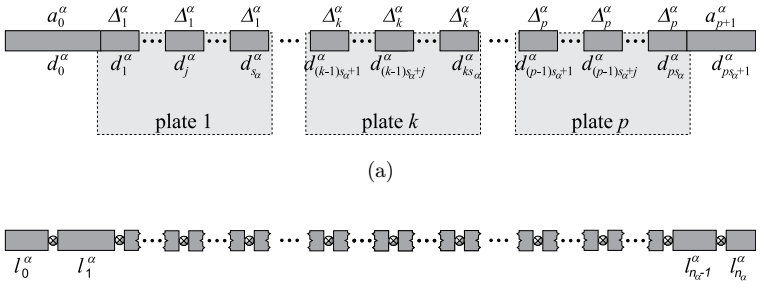

(a)

(b)

Fig. 7. Division of beams into rfe and sde: (a) primary and (b) secondary.

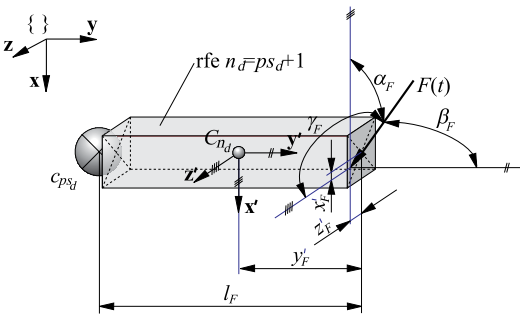

Fig. 8. Model of an impulse force inducing vibrations in the lower beam.

3. Preliminary Test Computations

Vibrations of electrodes have a nature of high-frequency processes. However, a direct comparison of such courses is not very effective. For this reason, the present study is focused on comparison of the peak values $W_{\max}$, median of peak values Me_s and the coefficient $\tilde{\Delta}_s$ of even distribution of peak values $W_{\max}(a_s)$ throughout the system. These values are defined by the following formulas:

$$W_{\max}(a_{s,i}) = \max_{0\le t\le T} |a_{s,i}|, \tag{3.1}$$

$$Me_s = median(W_{\max}(a_{s,i})), \tag{3.2}$$

$$\Delta_s = Me_s - \min_{0\le i\le n_p} (W_{\max}(a_{s,i})), \tag{3.3}$$

$$\tilde{\Delta}_s = \frac{\Delta_s - (\Delta_s)_{base}}{(\Delta_s)_{base}} \cdot 100\%, \tag{3.4}$$

where T is time of the analysis, i is index of the control point, n_p is the number of the control points, $(\Delta_s)_{base}$ is base values obtained numerically for the "classic" anvil position in the system (Fig. 4) and for angles of application of impulse force $\alpha_F = \gamma_F = 90^o, \beta_F = 0^o$ applied to the point $(x'_F, y'_F, z'_F) = (0, 0.5l_F, 0)$, Fig. 8. In the above equations $a_{s,i}$ can take one of the following values:

$$a_{s,i} = \begin{cases} a_{x,i} & -\text{acceleration in direction of the axis } \mathbf{x}, \\ a_{y,i} & -\text{acceleration in direction of the axis y}, \\ a_{n,i} = a_{z,i} & -\text{normal acceleration in the plane } \mathbf{xy}, \\ a_{t,i} = \sqrt{a_{x,i}^2 + a_{y,i}^2} & -\text{tangential accelration in the plane } \mathbf{xy}, \\ a_{c,i} = \sqrt{a_{x,i}^2 + a_{z,i}^2 + a_{y,i}^2} & -\text{total acceleration}, \end{cases}$$

and hence $s = \{x, y, t, n, c\}$. Simulations for the above-mentioned variants have been carried out for the following fixed parameters:

(i) force impulse: the time history is shown in Fig. 9(a);
(ii) integration step $h_c = 1 \times 10^{-5}$ s;

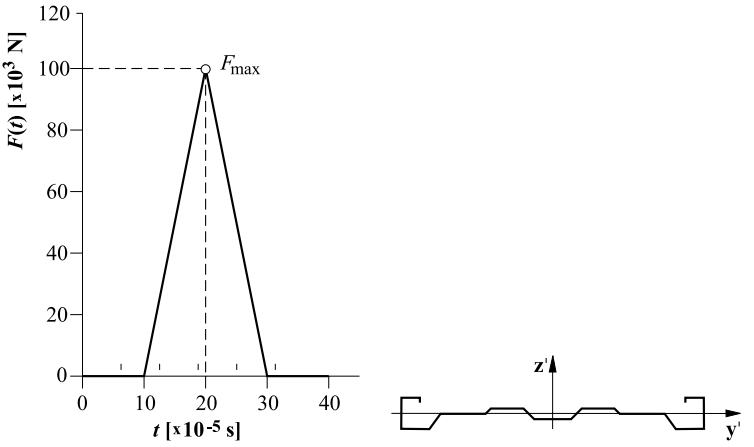

Fig. 9. Scheme of the system for tests: (a) course of the impulse force and (b) analyzed profile of electrodes.

(iii) density of discretization of the electrode strips $n_k = 200$;
(iv) simulation time $T = 2 \times 10^{-2}$ s;
(v) Young modulus $E = 2.06 \times 10^{11}$ Pa;
(vi) Poisson number $\nu = 0.3$.

Peak values $W_{\max}(a_s)$ of the tangential and normal component and total acceleration have been compared by taking 100 control levels spaced at 0.16 m. At each level the acceleration values have been determined in 225 points. No numbers were assigned to the points. The model presented in this study has been used to simulate vibrations induced by the impulse force demonstrated in Fig. 9(a).

In what follows the results of exemplary numerical simulations of the vibrations of a set of electrodes of the profile presented in Fig. 9(b) are illustrated and discussed. The analysis covered sets of 9 electrodes of the length of 16 m, made of rolled sheet and having the thickness of 1.5 mm.

3.1. *Analysis of the shift of the anvil beam*

The study of the impact of the position of the anvil beam on the distribution of accelerations in the system of electrodes is limited to the analysis of the cases presented in Fig. 10.

In the first case the beam (variant H16) is located at the bottom edge of electrodes (16 m below the suspension beam), and thus in the position applied mostly in the ESP produced in Poland (so called "classic" position). In successive cases the beam is raised 1 m up as compared to the previous case. The calculations are made for angles of application of the impulse force $\alpha_F = \gamma_F = 90^o, \beta_F = 0^o$ applied to the point $(x'_F, y'_F, z'_F) = (0, 0.5l_F, 0)$, Fig. 8. For clarity, the presentation of the maps of the peak values is limited to total accelerations. Figure 11 presents the map of peak

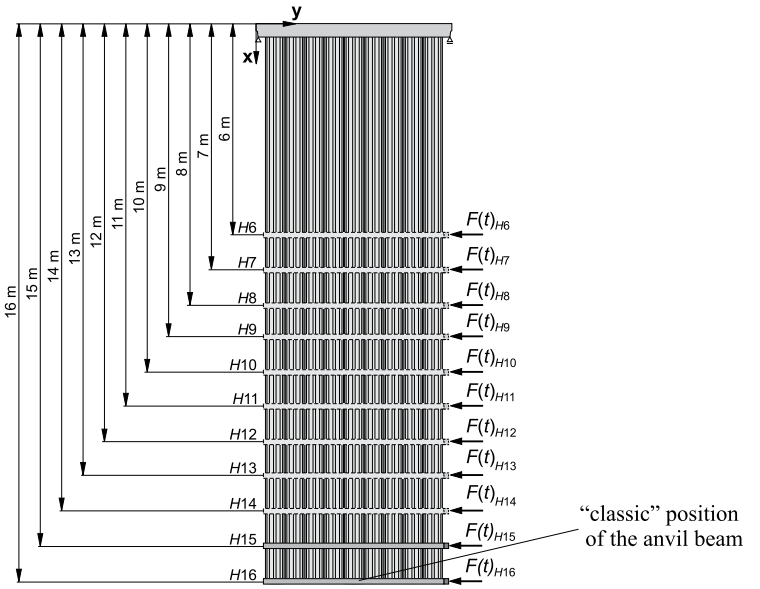

Fig. 10. Variants with a variable height of anvil beam position ($H6, \ldots, H16$).

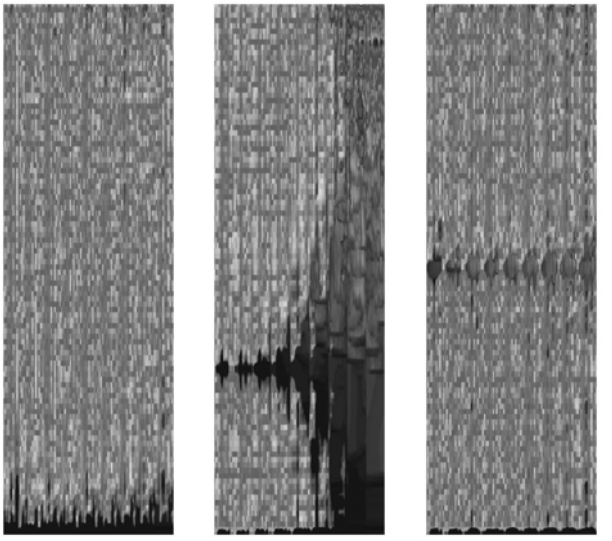

(a) (b) (c)

Fig. 11. Peak values $W_{\max}(a_c)$ of the total acceleration at time $t = 2 \times 10^{-2}$ s after the application of the impulse force regarding the position of the anvil beam: (a) $H16$, (b) $H11$ and (c) $H8$.

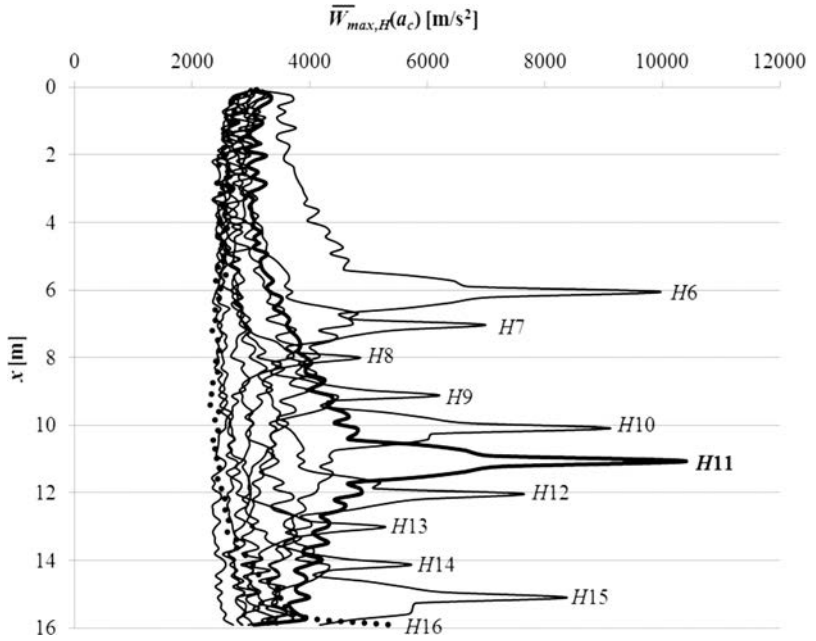

Fig. 12. Influence of the position of the anvil beam on the mean peak values $\bar{W}_{\max,H}(a_c)$ of control levels in the variants $H6, \ldots, H16$.

values $W_{max}(a_c)$ of total accelerations of the control points of the system, obtained during the simulation.

Based on the presented results it can be observed that the shift of the anvil beam toward the upper beam allows for a more even distribution of the peak values $W_{\max}$ (a_c) throughout the system. The quantitative assessment of the vibrations in the system is performed by comparing mean peak values $\bar{W}_{\max,H}(a_c)$ of control levels (Fig. 12) and mean peak levels $\bar{W}_{\max,H}(a_s)$ of the system of electrodes (Fig. 13).

The analysis of the values $\bar{W}_{\max,H}(a_c)$ from Fig. 12 helps to observe that the position H8 of the anvil beam allows for a more even distribution of peak values of accelerations in the system. On the other hand, in the position H11 the mean peak values of the quantities: $\bar{W}_{\max}(a_n)$ — normal component, $\bar{W}_{\max}(a_t)$ — tangential component and $\bar{W}_{\max}(a_c)$ — total acceleration are in this case the highest (Fig. 13).

3.2. *Analysis of the impulse force loading*

The study of the influence of the impulse force loading on vibrations of the collecting electrode system is limited to the analysis of the cases presented in Tables 1–3. In all cases the anvil beam is located at the bottom edge of electrodes, 16 m below the suspension beam (like in variant $H16$ in Fig. 10).

The quantitative assessment of the vibrations in the system is performed by comparing mean peak levels $\bar{W}_{\max}(a_s)$ of the system of electrodes as well as median

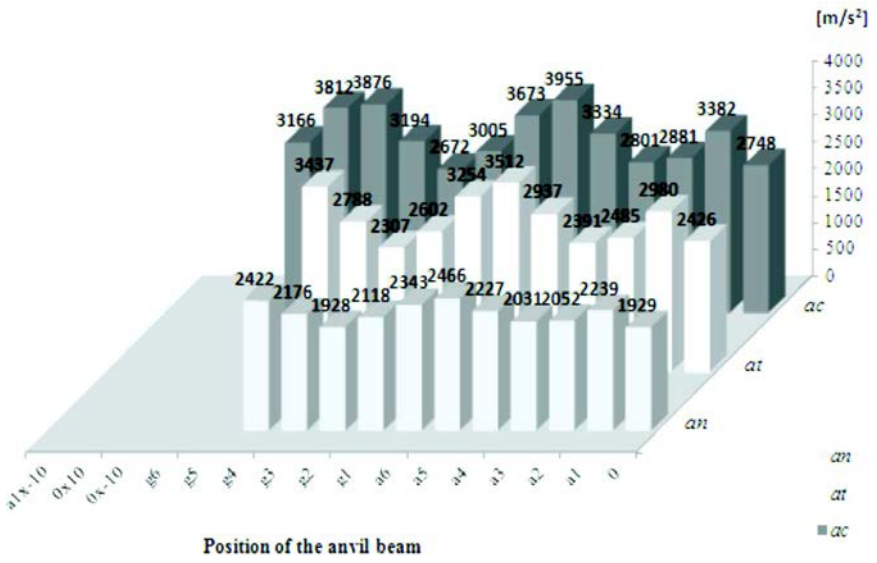

Fig. 13. Influence of the position of the anvil beam on mean peak values $\bar{W}_{\max}(a_s)$ of the electrode system in the variants $H6, \ldots, H16$.

Me_s of peak values $W_{\max}(a_{s,i})$ and the coefficient $\tilde{\Delta}_s$ of even distribution of peak values $W_{\max}(a_s)$ throughout the system. Results obtained from variant A5 (the "classic" position of an anvil beam in the system) are the base values. All other results of numerical simulations are compared with these results.

The analysis of the values $\bar{W}_{max}(a_s)$ from Fig. 14 helps to observe that minor changes of angles α_F and γ_F ($90^o \pm 5^o$, cases: $A2, \ldots, A8$ and $G1, \ldots, G6$) do not significantly affect the values of the total acceleration and its normal and tangent components (the results differ by less than 1.5%). At a similar way changes the

Table 1. The variants of direction of impulse force as function of angle α_F and $\gamma_F = 90^o = const$ ($\beta_F = (90^o - \alpha_F)$ and the point of impulse force application is $(x'_F, y'_F, z'_F) = (0, 0.5l_F, 0)$).

Variant ID:	A1	A2	A3	A4	A5	A6	A7	A8	A9	A10
$\alpha_F(^o)$:	80	85	87	89	90	91	93	95	100	120

Table 2. The variants of direction of impulse force as function of angle γ_F and $\alpha_F = 90^o = const$ ($\beta_F = (90^o - \gamma_F)$ and the point of impulse force application is $(x'_F, y'_F, z'_F) = (0, 0.5l_F, 0)$).

Variant ID:	G1	G2	G3	G4	G5	G6
$\gamma_F(^o)$:	85	87	89	90	91	93

Table 3. The variants of the point $(x'_F, y'_F = 0.5l_F, z'_F = 0)$ of impulse force application and constant values of angles $\alpha_F = \gamma_F = 90^o = const$, $\beta_F = 0^o$.

Variant ID:	P1	P2	P3
$x'_F(m)$:	−0.02	−0.01	0.01

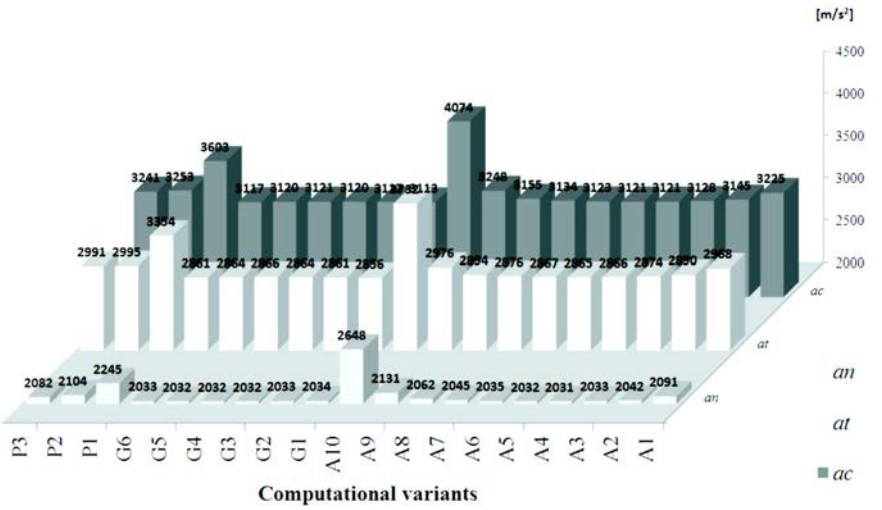

Fig. 14. Influence of the impulse force loading on mean peak values $\bar{W}_{max}(a_s)$ of the electrode system in the variants of the direction of impulse force: $A1, \ldots, A10$ and $G1, \ldots, G6$, and different points of the impulse force application: $P1$, $P2$, $P3$.

coefficient $\tilde{\Delta}_s$ of even distribution of the peak values of the accelerations in the system. The results reported in Table 4 differ by less than 5.5%. These observations allow to assume that inaccuracies in mounting of rapping system have no significant influence on the values and even distribution of acceleration in the collecting electrode system.

Moreover, the analysis of the values $\bar{W}_{max}(a_s)$ shown in Fig. 14 helps to observe that changes of α_F angle (over $90^o \pm 10^o$, cases: $A1$, $A9$, $A10$) or x'_F coordinate of the point of the impulse force application ($x'_F > 0.01$ m, case $P1$) significantly affect the values of the total acceleration and its normal and tangent components. The results differ by more than 30% in $A1$ variant and by more than 10% in $P1$. Differences of the $\tilde{\Delta}_s$ values of even distribution of the peak values of the accelerations in the system (Table 4) are even greater, and the results differ by more than 80% in the case of normal acceleration. These observations allow us to assume that inaccuracies in mounting of rapping system have no significant influence on the values and even distribution of acceleration in the collecting electrode system. That means,

Table 4. Values of median Me_s of peak values $W_{max}(a_{s,i})$ and the coefficient $\tilde{\Delta}_s$ of even distribution of peak values $W_{max}(a_s)$throughout the system.

Variant ID	Me_c [m/s^2]	$\tilde{\Delta}_c$ (%)	Me_t [m/s^2]	$\tilde{\Delta}_t$ (%)	Me_n [m/s^2]	$\tilde{\Delta}_n$ (%)
A1	2977	1.5	2797	8.2	1852	−0.1
A2	2902	−1.2	2722	1.5	1817	−5.2
A3	2886	−1.1	2705	1.0	1811	−4.1
A4	2880	0.0	2698	0.3	1806	−1.3
A5	2879	0.0	2697	0.0	1808	0.0
A6	2881	0.9	2700	−0.4	1809	−0.1
A7	2892	1.4	2708	−1.3	1815	1.3
A8	2910	1.1	2726	−2.3	1830	2.6
A9	3002	−1.5	2810	9.9	1882	14.9
A10	3723	16.7	3488	63.7	2257	82.1
G1	2871	−1.8	2690	0.4	1807	0.6
G2	2877	−0.8	2695	0.3	1807	0.4
G3	2879	−0.1	2697	0.1	1808	−0.7
G4	2879	0.5	2697	−0.2	1808	−0.3
G5	2873	0.8	2693	−0.7	1802	−0.7
G6	2870	−0.3	2690	−1.2	1803	−0.3
P1	3338	19.7	3164	51.9	1970	21.3
P2	3003	2.3	2828	5.5	1855	2.5
P3	2991	3.4	2819	12.6	1848	−3.9

displacement of the point of application of force pulse, which is a result of connecting the force sensor to the anvil, should be always taken into account, when the impulse force is measured.

4. Concluding Remarks

In general the process of inducing vibrations and their propagation in the electrode system is a resultant of many factors. It depends not only on the size of impulse force, but also on physical, geometrical and structural parameters of all system components. The experiments carried out in the present study imply the following remarks:

(i) The values of total acceleration cannot determine the selection of a profile of electrodes as the sole factor. Only the combined use of indicators of the assessment of peak values of all the components of acceleration yields the optimal variant.

(ii) The position (height) of anvil beam installation in the system of electrodes may affect the size and distribution of the generated vibrations, as well as the time of their propagation. As shown in the study, the classical position of the rod in the system is not the most favorable.

(iii) The shift of rapping rod towards the upper beam does not cause a significant increase in the acceleration values, but it can contribute to their more even distribution.

(iv) Inaccuracies in mounting of rapping system have no significant influence on the values and even distribution of acceleration in the collecting electrode system as long as they make minor changes of the angles of impulse force direction and/or position of its point of application.

The results of test computations demonstrate that intuition of engineers responsible for the design of electrodes is generally correct. The location of the anvil beam in a position other than the classic one would require significant changes in current structures, encountering a number of technical difficulties.

References

1. M. C. R. Falaguasta, J. Steffens, E. E. Valdes and J. R. Coury, Overall collection efficiency of a plate-wire electrostatic precipitator operating on the removal of PM2.5, *Lat. Am. Appl. Res.* **38**(2) (2008) 179–186.
2. D. Brocilo, J. Podlinski, J. S. Chang, J. Mizeraczyk and R. D. Findlay, Electrode geometry effects on the collection efficiency of submicron and ultrafine dust particles in spikeplate electrostatic precipitators, *J. Phys. Conf. Ser.* **142**(012032) (2008) 1–6.
3. M. Neuendorfer, Electrode cleaning systems: Optimizing rapping energy and rapping control, *Environ. Int.* **6**(1–6) (1981) 279–287.
4. M. R. Talaie, Mathematical modeling of wireduct singlestage electrostatic precipitators, *J. Hazard. Mater.* **124**(13) (2005) 44–52.
5. X. F. Yang, Y. M. Kang and K. Zhong, Effects of geometric parameters and electric indexes on the performance of laboratory–scale electrostatic precipitators, *J. Hazard. Mater.* **169**(13) (2009) 941–947.
6. J. K. Lee, J. H. Ku, J. E. Lee, S. C. Kim, Y. C. Ahn, J. H. Shin and S. H. Choung, An experimental study of electrostatic precipitator plate rapping and reentrainment, in *Proc. ICESP VII*, Kyongju, Korea (September, 1998), pp. 20–25.
7. S. L. Franci, A. Bck and P. Johansson, Reduction of rapping losses to improve ESP performance, *Electrostatic Precipitationed*, K. Yan (Springer, 2009), pp. 45–49, doi: 10.1007/978-3-540-89251-9-6.
8. P. Wanjari and K. M. Narkar, Design modification of rapping system to improve the dust collection efficiency of electrostatic precipitator, *Int. J. Innovat. Res. Sci. Eng. Technol.* **3** (8) (2014) 15130–15136.
9. I. Adamiec-Wójcik, A. Nowak and S. Wojciech, Comparison of methods for vibration analysis of electrostatic precipitators, *Acta Mech. Sinica* **1**(27) (2011) 72–79.
10. I. Adamiec-Wójcik, Modelling of systems of collecting electrodes of electrostatic precipitators by means of the rigid finite element method, *Arch. Mech. Eng.* **58**(1) (2011) 27–47, doi: 10.2478/v10180-011-0002-x.
11. I. Adamiec-Wójcik, J. Awrejcewicz, A. Nowak and S. Wojciech, Vibration analysis of collecting electrodes by means of the hybrid finite element method, *Math. Probl. Eng.* **832918** (2014), doi: 10.1155/2014/832918.
12. A. Nowak, Modelling and measurements of vibrations of collecting electrodes of dry electrostatic precipitators, Habilitation Thesis, University of Bielsko-Biała (Bielsko-Biała, 2011).
13. A. Nowak, P. Nowak and J. Awrejcewicz, Influence of position of an anvil beam on vibrations of collecting electrodes, *Dynamical Systems: Mathematical and Numerical Approaches*, eds. J. Awrejcewicz, M. Kaźmierczak, J. Mrozowski and P. Olejnik (Łódź, 2015), pp. 391–402.

14. J. Kruszewski, W. Gawroński, E. Wittbrodt, F. Najbar and S. Grabowski, *The Rigid Finite Element Method* (Arkady, Warsaw, 1975).
15. W. Gawroński, J. Kruszewski, W. Ostachowicz, J. Tarnowski and E. Wittbrodt, *The Finite Element Method in Dynamics of Structures* (Arkady, Warsaw, 1984).
16. M. Abramowicz, Modeling of free vibration and identyfication of parameters of steel-concrete composite beams, Ph.D. Thesis, West Pomeranian University of Technology in Szczecin, Szczecin (2014).
17. I. Adamiec-Wójcik and S. Wojciech, Application of a rigid finite element method in dynamic analysis of plane manipulators, *Mech. Mach. Theory* **28**(3) (1993) 327–334.